

Context-dependent computation by recurrent dynamics in prefrontal cortex

Valerio Mante^{1†*}, David Sussillo^{2*}, Krishna V. Shenoy^{2,3} & William T. Newsome¹

Prefrontal cortex is thought to have a fundamental role in flexible, context-dependent behaviour, but the exact nature of the computations underlying this role remains largely unknown. In particular, individual prefrontal neurons often generate remarkably complex responses that defy deep understanding of their contribution to behaviour. Here we study prefrontal cortex activity in macaque monkeys trained to flexibly select and integrate noisy sensory inputs towards a choice. We find that the observed complexity and functional roles of single neurons are readily understood in the framework of a dynamical process unfolding at the level of the population. The population dynamics can be reproduced by a trained recurrent neural network, which suggests a previously unknown mechanism for selection and integration of task-relevant inputs. This mechanism indicates that selection and integration are two aspects of a single dynamical process unfolding within the same prefrontal circuits, and potentially provides a novel, general framework for understanding context-dependent computations.

Our interactions with the world are inherently flexible. Identical sensory stimuli, for example, can lead to very different behavioural responses depending on ‘context’, which includes goals, previous expectations about upcoming events, and relevant past experiences^{1,2}. Animals can switch rapidly between behavioural contexts, implying the existence of rapid modulation, or ‘gating’, mechanisms within the brain that select relevant sensory information for decision-making and action. A large attention literature suggests that relevant information is selected by top-down modulation of neural activity in early sensory areas^{3–8}, which may take the form of modulation of firing rates^{3,5–7}, or modulation of response synchrony within or across areas^{4,5,8}. The top-down signals underlying such ‘early’ modulations of sensory activity arise, in part, from prefrontal cortex (PFC)^{2,5}, which is known to contribute to representing and maintaining contextual knowledge, ignoring irrelevant information, and suppressing inappropriate actions^{1,2,9,10}. These observations have led to the hypothesis that early selection may account for the larger effect of relevant as compared to irrelevant sensory information on contextually sensitive behaviour.

Here we test this hypothesis with a task requiring context-dependent selection and integration of visual stimuli. We trained two macaque monkeys (A and F) to perform two different perceptual discriminations on the same set of visual stimuli (Fig. 1). The monkeys were instructed by a contextual cue to either discriminate the direction of motion or the colour of a random-dot display, and to report their choices with a saccade to one of two visual targets (Fig. 1a). While monkeys performed this task, we recorded extracellular responses from neurons in and around the frontal eye field (Extended Data Fig. 1a, f), an area of PFC involved in the selection and execution of saccadic eye movements^{11,12}, the control of visuo-spatial attention¹³, and the integration of information towards visuomotor decisions^{12,14}.

We found no evidence that irrelevant sensory inputs are gated, or filtered out, before the integration stage in PFC, as would be expected from early selection mechanisms^{3–8}. Instead, the relevant input seems to be selected late, by the same PFC circuitry that integrates sensory evidence towards a choice. Selection within PFC without previous

gating is possible because the representations of the inputs, and of the upcoming choice, are separable at the population level, even though they are deeply entwined at the single neuron level. An appropriately trained recurrent neural network model reproduces key physiological observations and suggests a new mechanism of input selection and integration. The mechanism reflects just two learned features of a dynamical system: an approximate line attractor and a ‘selection vector’, which are only defined at the level of the population. The model mechanism is readily scalable to large numbers of inputs, indicating a general solution to the problem of context-dependent computation.

Behaviour and single-unit responses

The monkeys successfully discriminated the relevant sensory evidence in each context, while largely ignoring the irrelevant evidence (Fig. 1c–f, monkey A; Extended Data Fig. 2a–d, monkey F). To vary the difficulty of the discrimination, we changed the strength of the motion and colour signals randomly from trial to trial (Fig. 1b). In the motion context, the choices of the monkeys depended strongly on the direction of motion of the dots (Fig. 1c), whereas the choices depended only weakly on colour in the same trials (Fig. 1d). The opposite pattern was evident in the colour context: the now relevant colour evidence exerted a large effect on choices (Fig. 1f) whereas motion had only a weak effect (Fig. 1e).

As is common in PFC^{1,2,15–18}, the recorded responses of single neurons appeared to represent several different task-related signals at once, including the monkey’s upcoming choice, the context, and the strength of motion and colour evidence (Extended Data Figs 1 and 3). Rather than attempting to understand the neural mechanism underlying selective integration by studying the responses of single PFC neurons, we focussed on analysing the responses of the population as a whole. To construct population responses, we pooled data from both single and multi-unit recordings, which yielded equivalent results. The great majority of units were not recorded simultaneously, but rather in separate sessions. Units at all recording locations seemed to contribute to the task-related signals analysed below (Extended Data Fig. 1) and were thus combined.

¹Howard Hughes Medical Institute and Department of Neurobiology, Stanford University, Stanford, California 94305, USA. ²Department of Electrical Engineering and Neurosciences Program, Stanford University, Stanford, California 94305, USA. ³Departments of Neurobiology and Bioengineering, Stanford University, Stanford, California 94305, USA. †Present address: Institute of Neuroinformatics, University of Zurich/ETH Zurich, CH-8057 Zurich, Switzerland.

*These authors contributed equally to this work.

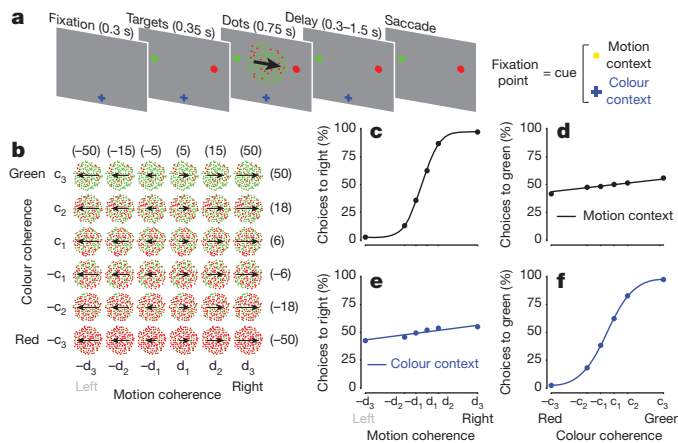


Figure 1 | Behavioural task and psychophysical performance. **a**, Task structure. Monkeys were instructed by a contextual cue to either discriminate the motion or the colour of a random-dot stimulus, and indicate their choice with a saccade to one of two targets. Depending on context, monkeys were rewarded for choosing the target matching the prevalent direction of motion (motion context) or the prevalent colour (colour context) of the random dots. Context was indicated by the shape and colour of the fixation point; offset of the fixation point was the ‘go cue’, signalling the monkey to indicate its choice via the operant saccade. **b**, Stimulus set. The motion and colour coherence of the dots was chosen randomly on each trial. We slightly varied the coherence values on each day, to equate performance across contexts and sessions (numbers in parentheses: average coherences (%) across sessions for monkey A). **c–f**, Psychophysical performance for monkey A in the motion (top) and colour contexts (bottom), averaged over 80 recording sessions (163,187 trials). Performance is shown as a function of motion (left) or colour (right) coherence in each behavioural context. The curves are fits of a behavioural model.

Overall, we analysed 388 single-unit and 1,014 multi-unit responses from the two monkeys.

State space analysis

To study how the PFC population as a whole dynamically encodes the task variables underlying the monkeys’ behaviour, we represent population responses as trajectories in neural state space^{17,19–25}. Each point in state space corresponds to a unique pattern of neural activations across the population. Because activations are dynamic, changing over time, the resulting population responses form trajectories in state space.

We focussed our analyses on responses in a specific low-dimensional subspace that captures across-trial variance due to the choice of the monkey (choice 1 or 2), the strength and direction of the motion evidence, the strength and direction of the colour evidence, and context (motion or colour). We estimated this task-related subspace in two steps (Supplementary Information). First, we used principal component analysis (PCA) to obtain an unbiased estimate of the most prominent features (that is, patterns of activations) in the population response. To ‘de-noise’ the population responses, we restricted subsequent analyses to the subspace spanned by the first 12 principal components. Second, we used linear regression to define the four orthogonal, task-related axes of choice, motion, colour and context. The projection of the population response onto these axes yields de-mixed estimates of the corresponding task variables, which are mixed both at the level of single neurons (Extended Data Fig. 3) and at the level of individual principal components (Extended Data Fig. 4c, g; see also ref. 26).

This population analysis yields highly reliable average response trajectories (Fig. 2 and Extended Data Fig. 4q, r) that capture both the temporal dynamics and the relationships among the task variables represented in PFC. In particular, four properties of the population responses provide fundamental constraints on the mechanisms of selection and integration underlying behaviour in our task.

First, integration of evidence during presentation of the random dots corresponds to a gradual movement of the population response

in state space along the axis of choice (Fig. 2a, f). In both contexts, the trajectories start from a point in state space close to the centre of the plots (‘dots on’, purple point), which corresponds to the pattern of population responses at baseline. During the dots presentation the responses then quickly move away from this baseline level, along the axis of choice (red line; Fig. 2a, f). Overall, the population response moves in opposite directions on trials corresponding to the two different saccade directions (Fig. 2, choice 1 versus choice 2). The projection of the population response onto the choice axis (Extended Data Fig. 5b, f) is largely analogous to the ‘choice-predictive’ signals that have been identified in past studies as approximate integration of evidence during direction discrimination tasks²⁷.

Second, the sensory inputs into PFC produce patterns of population responses that are very different from those corresponding to either choice, meaning that these signals are separable at the level of the population. Indeed, the population response does not follow straight paths along the choice axis, but instead forms prominent arcs away from it (Fig. 2a, f). The magnitude of each arc along the axes of motion or colour reflects the strength of the corresponding sensory evidence (see scale), whereas its direction (up or down) reflects the sign of the evidence (towards choice 1 or 2, filled or empty symbols, respectively). Whereas the integrated evidence continues to be represented along the axis of choice even after the disappearance of the random dots (‘dots off’), the signals along the axes of motion and colour are transient—the arcs return to points near the choice axis by the time of dots offset. These signals thus differ from integrated evidence both in terms of the corresponding patterns of activation and in their temporal profile. For these reasons, we interpret them as ‘momentary evidence’ from the motion and colour inputs in favour of the two choices. This interpretation is also consistent with the observed population responses on error trials, for which the momentary evidence points towards the chosen target, but is weaker than on correct trials (Extended Data Fig. 5c, d; red curves).

Third, context seems to have no substantial effect on the direction of the axes of choice, motion and colour, and only weak effects on the strength of the signals represented along these axes. When estimated separately during the motion and colour contexts, the two resulting sets of axes span largely overlapping subspaces (see Supplementary Table 1); thus, a single set of three axes (the red, black and blue axes in Fig. 2a–f, estimated by combining trials across contexts) is sufficient to capture the effects of choice, motion and colour on the population responses in either context. A comparison of the population responses across contexts (Fig. 2a–c versus d–f) reveals that a single, stable activity pattern is responsible for integrating the relevant evidence in both contexts (the choice axis), while similarly stable activity patterns represent the momentary motion and colour evidence in both contexts (motion and colour axes). Notably, motion and colour inputs result in comparable deflections along the motion and colour axes, respectively, whether they are relevant or not (compare Fig. 2a to d and f to c).

Fourth, although the directions of the axes of choice, motion and colour are largely invariant with context, their location in state space is not. The responses during the motion and colour contexts occupy different parts of state space, and the corresponding trajectories are well separated along the axis of context (Extended Data Fig. 6a, b).

Comparison to models of selection and integration

These properties of the population responses, which are summarized schematically in Fig. 3a, can be compared to the predictions of current models of context-dependent selection and integration (Fig. 3b–d). We first focussed on three fundamentally different mechanisms of selection that could each explain why the motion input, for example, influences choices in the motion context (Fig. 3, top row) but not in the colour context (Fig. 3, bottom row). In the framework of our task the three models predict population responses that differ substantially

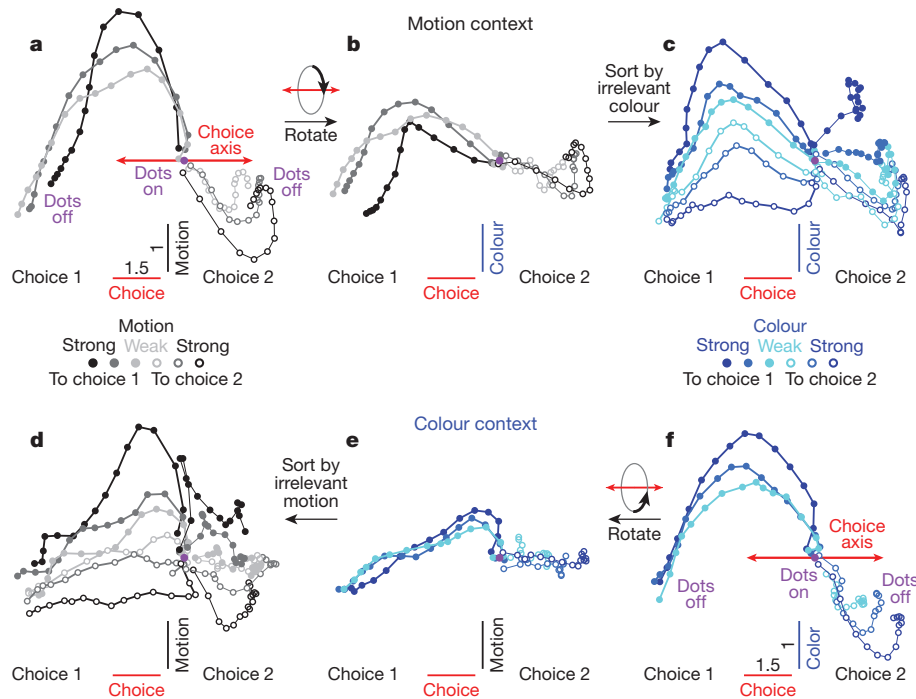


Figure 2 | Dynamics of population responses in PFC. The average population response for a given condition and time is represented as a point in state space. Responses from correct trials only are shown from 100 ms after dots onset (dots on, purple circle) to 100 ms after dots offset (dots off) in 50-ms steps, and are projected into the three-dimensional subspace capturing the variance due to the monkey's choice (along the choice axis), and to the direction and strength of the motion (motion axis) and colour (colour axis) inputs. Units are arbitrary; components along the motion and colour axes are enhanced relative to the choice axis (see scale bars in a, f). Conditions (see colour bars) are defined based on context (motion context, top; colour context, bottom), on the location of the chosen target (choice 1 versus choice 2) and either on the direction and strength of the motion (grey colours) or the colour input (blue colours). Here, choice 1 corresponds to the target in the response field of the recorded neurons. The direction of the colour input does not refer to

the colour of the dots per se (red or green), but to whether the colour points towards choice 1 or choice 2 (see Supplementary Information, section 6.4, for a detailed description of the conditions). **a**, Effect of choice and the relevant motion input in the motion context, projected onto the axes of choice and motion. **b**, Same data as in a, but rotated by 90° around the axis of choice to reveal the projection onto the axis of colour. **c**, Same trials as in b, but re-sorted according to the direction and strength of the irrelevant colour input. **d–f**, Responses in the colour context, analogous to a–c. Responses are averaged to show the effects of the relevant colour (e, f) or the irrelevant motion input (d). For relevant inputs (a, b and e, f), correct choices occur only when the sensory stimulus points towards the chosen target (3 conditions per chosen target); for irrelevant inputs (c, d), however, the stimulus can point either towards or away from the chosen target on correct trials (6 conditions per chosen target).

from each other (Fig. 3b–d), and can thus be validated or rejected by our PFC recordings (Fig. 3a).

The first model (Fig. 3b) is based on two widely accepted hypotheses about the mechanisms underlying selection and integration of evidence. First, it assumes that inputs are selected early^{3–8}, such that a given input drives PFC responses when relevant (grey arrow in Fig. 3b, top), but is filtered out before reaching PFC when irrelevant (no grey arrow in Fig. 3b, bottom). Second, it assumes that the relevant input directly elicits a pattern of activation in PFC resembling the pattern corresponding to a choice (the grey arrow in Fig. 3b, top, points along the axis of choice), as would be expected by current models of integration^{28,29}.

Both hypotheses are difficult to reconcile with the recorded PFC responses. Whereas the strength of each input is reduced when it is irrelevant compared to when it is relevant, the magnitude of the observed reduction seems too small to account for the behavioural effects. For instance, irrelevant motion of high coherence (Fig. 2d, black) elicits a larger deflection along the motion axis (relative to baseline, purple dot, Fig. 2d) than relevant motion of intermediate coherence (Fig. 2a, dark grey). Yet the former has almost no behavioural effect (Fig. 1e), whereas the latter has a large behavioural effect (Fig. 1c). The analogous observation holds for the colour input (Figs 2c, f and 1d, f), strongly suggesting that the magnitude of the momentary evidence alone does not determine whether the corresponding input is integrated. Furthermore, the actual momentary motion input is represented along a direction that has little overlap

with the choice axis, resulting in curved trajectories (Fig. 3a) that differ markedly from the straight trajectories predicted by the early selection model (Fig. 3b).

The observed PFC responses also rule out two additional models of selection presented in Fig. 3. In the absence of early selection, a motion input might be selected within PFC by modifying the angle between the choice and motion axes (that is, the similarity between patterns of neural activity representing choice and momentary motion evidence) across contexts. This angle could be modified either by changing the direction of the motion axis between contexts while keeping the choice axis fixed (Fig. 3c), or vice versa (Fig. 3d). In both cases, the motion input would elicit movement of the population along the axis of choice in the motion context (top row), but not in the colour context (bottom row), as the motion and choice axes have little or no overlap in the colour context. At the single neuron level, variable axes that change direction across contexts would be reflected as complex, nonlinear interactions between context and the other task variables, which have been proposed in some task-switching models^{30,31}. However, our data (Figs 2 and 3a) lend little support for variable choice (Fig. 3d) or input (Fig. 3c) axes. More generally, the PFC data from monkey A rule out any model of integration for which the degree of overlap between the direction of the momentary evidence and the axis of choice determines how much the corresponding input affects behaviour.

The representation of task variables in PFC of monkey F replicates all but one key feature observed in monkey A. Most importantly, population responses along the choice and motion axes (Extended

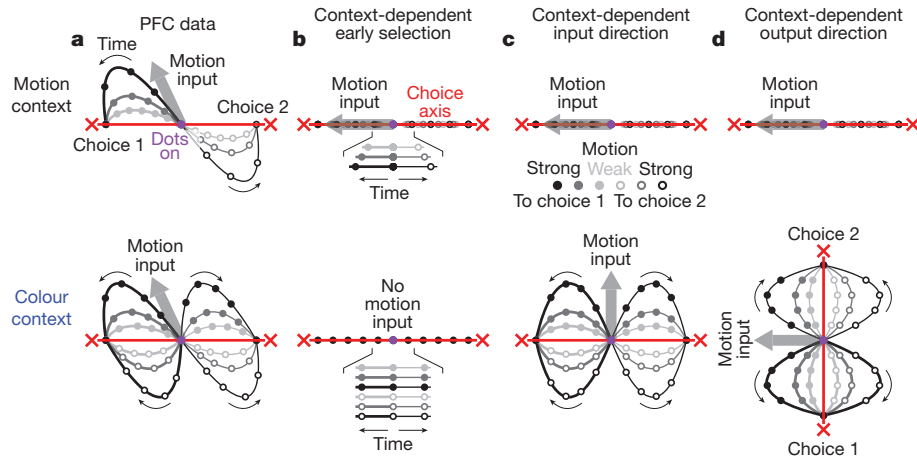


Figure 3 | Models of selective integration inconsistent with PFC responses. Schematic representation of population responses observed in PFC (a) and expected by several models of selective integration (b–d). The models differ from the PFC responses with respect to the relative directions and context dependence of the choice axis (red lines) and the inputs (thick grey arrows; only motion input is shown). The relevant input is integrated as movement along the choice axis towards one of two choices (red crosses). A motion input towards choice 1 ‘pushes’ the responses along the direction of the grey arrow (towards choice 2: opposite direction). Same conditions as in Fig. 2a (motion context, top) and Fig. 2d (colour context, bottom). As in Fig. 2a and d, a single two-dimensional subspace (which contains the choice axis and motion input) is used to represent responses from both contexts. **a**, Idealized schematic of the actual PFC trajectories shown in Fig. 2a, d. Both the choice axis and motion input are stable between contexts. The motion input pushes the population response away from the choice axis. **b**, Early selection model. When relevant

(top), the motion input pushes the population response along the choice axis. When irrelevant (bottom), the motion input is filtered out before reaching PFC (no thick grey arrow) and thus exerts no effect on choice. All trajectories fall on top of each other in both contexts, but the rate of movement along the choice axis increases with motion strength only in the motion context (insets show enlarged trajectories distributed vertically for clarity). **c**, Context-dependent input direction. Motion input direction varies between contexts, whereas the choice axis is stable. Inputs are not filtered out before PFC; rather, they are selected on the basis of their projection onto the choice axis. **d**, Context-dependent output direction. Similar selection mechanism to **c**, except that the choice axis varies between contexts, whereas the motion input is stable. The effects of the motion input on PFC responses in both monkeys (schematized in **a**) and the effects of the colour input in monkey A are inconsistent with predictions of the three models in **b–d** (respectively, Fig. 2a, d; Extended Data Fig. 7a,d; Fig. 2f, c).

Data Fig. 7a, d) closely match those observed in monkey A (Fig. 2a, d); thus, physiological data from both monkeys are consistent in rejecting current models of selection and integration of motion inputs (Fig. 3b–d). The colour signal in monkey F, however, is equivocal. On the one hand, the representation of the colour input closely resembles that of a choice (Extended Data Fig. 1g, i), as expected from the early selection model described above (Fig. 3b). On the other hand, the colour input is also weakly represented along the colour axis in both contexts (vertical displacement of trajectories, Extended Data Fig. 7c, f). For the colour input in monkey F, therefore, we cannot with confidence accept or reject the early selection model. Finally, as in monkey A, context is represented in monkey F along a separate axis of context (Extended Data Fig. 6c, d).

In summary, the population responses in both monkeys are difficult to reconcile with current models of selection and integration (see also Extended Data Fig. 8). Rather, the selective integration of the motion input in monkeys A and F, and of the colour input in monkey A, must rely on a mechanism for which the very same input into PFC leads to movement along a fixed axis of choice in one context but not another.

Recurrent network model of selection and integration

To identify such a mechanism, we trained a network of recurrently connected, nonlinear neurons³² to solve a task analogous to the one solved by the monkeys (Fig. 4). Notably, we only defined ‘what’ the network should do, with minimal constraints on ‘how’ it should do it^{32–34}. Thus, the solution achieved by the network is not hand-built into the network architecture. On each trial, neurons in the network receive two independent sensory inputs that mimic the momentary evidence for motion and colour in a single random dot stimulus. The network also receives a contextual input that mimics the contextual signal provided to the monkeys, instructing the network to discriminate either the motion or the colour input. The network activity is read out by a single linear read-out, corresponding to a weighted sum

over the responses of all neurons in the network (see Supplementary Information). As in PFC, the contextual input does not affect the strength of the sensory inputs—selection occurs within the same network that integrates evidence towards a decision.

We trained the network³⁵ to make a binary choice on each trial—an output of +1 at the end of the stimulus presentation if the relevant evidence pointed leftward, or a –1 if it pointed rightward. After training, the model qualitatively reproduces the monkeys’ behaviour,

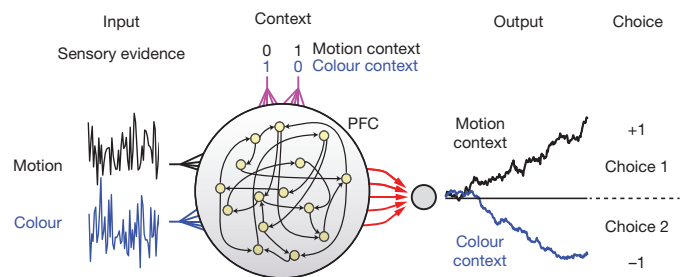


Figure 4 | A neural network model of input selection and integration. PFC is modelled as a network of recurrently connected, nonlinear, rate neurons that receive independent motion, colour and contextual inputs. The network is fully recurrently connected, and each unit receives both motion and colour inputs as well as two inputs that indicate context. At each time step, the sensory inputs are drawn from two normal distributions, the means of which correspond to the average strengths of the motion and colour evidence on a given trial. The contextual inputs take one of two values (0 or 1), which instruct the network to discriminate either the motion or the colour input. The network is read out by a single linear read-out, corresponding to a weighted sum over the responses of all neurons (red arrows). We trained the network (with back-propagation³⁵) to make a binary choice, that is, to generate an output of +1 at the end of the stimulus presentation if the relevant evidence pointed towards choice 1, or a –1 if it pointed towards choice 2. Before training, all synaptic strengths were randomly initialized.

confirming that the model solves the selection problem at the ‘behavioural’ level (Extended Data Fig. 2e–h).

We first analysed model population trajectories in the subspace spanned by the axes of choice, motion and colour, and found that they reproduce the four main features of the PFC population responses discussed above (Fig. 5 and Extended Data Fig. 9a–g). First, integration of evidence corresponds to gradual movement of the population response along the choice axis. Second, momentary motion and colour evidence ‘push’ the population away from the choice axis, resulting in trajectories that are parametrically ordered along the motion and colour axes. Third, the direction of the axes of choice, motion and colour are largely invariant with context, as are the strength of the motion and colour inputs, as these are not gated before entering the network. Fourth, the trajectories during motion and colour contexts are separated along the axis of context (Extended Data Fig. 9f, g). Model and physiological dynamics differ markedly in one respect—signals along the input axes are transient in the physiology, but not in the model, yielding PFC trajectories that curve back to the choice axis before the end of the viewing interval (compare Figs 5a, f to 2a, f). This difference suggests that the sensory inputs to PFC are attenuated after a decision is reached. Additional differences between the model and the physiological dynamics can be readily explained by previously proposed imperfections in the evidence integration process, such as ‘urgency’ signals^{36,37} or instability in the integrator³⁸ (Extended Data Fig. 10).

A novel mechanism of selective integration

We then ‘reverse engineered’ the model³³ to discover its mechanism of selective integration. The global features of the model activity are easily explained by the overall arrangement of fixed points of the dynamics³³ (Fig. 5), which result from the synaptic connectivity learned during training. Fixed points (small red crosses) correspond to patterns of neuronal activations (that is, locations in state space) that are stable when the sensory inputs are turned off. First, we found that the model generates a multitude of fixed points, which are approximately arranged to form two lines along the choice axis. The two sets of fixed points are separated along the axis of context (Extended Data Fig. 9f, g) and never exist together—one exists in the motion context (Fig. 5a–c), the other in the colour context (Fig. 5d–f).

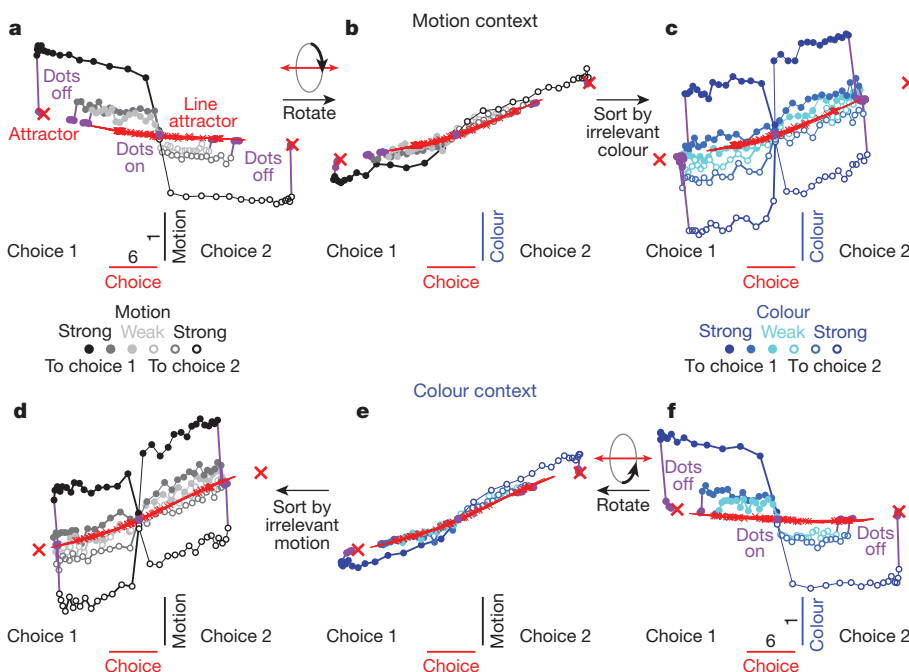


Figure 5 | Model dynamics and fixed points analysis. a–f, Dynamics of model population responses, same conventions as in Fig. 2. Responses are projected into the three-dimensional subspace spanned by the axes of choice, motion and colour (defined here based on the model synaptic weights, see Supplementary Information, section 7.6). Movement along the choice axis corresponds to integration of evidence, and the motion and colour inputs deflect the trajectories along the corresponding input axes. Fixed points of the dynamics (red crosses) were computed separately for motion (a–c) and colour contexts (d–f) in the absence of sensory inputs (see Supplementary Information, section 7.5). The fixed points are ‘marginally stable’ (that is, one eigenvalue of the linearized dynamics is close to zero, whereas all others have strongly negative real parts; see Supplementary Information). The locally computed right zero-eigenvectors (red lines) point to the neighbouring fixed points, which thus approximate a line attractor in each context. After the inputs are turned off (dots off, purple data points and lines) the responses relax back towards the line attractor. Each line attractor ends in two ‘stable’ attractors (that is, all eigenvalues have strongly negative real parts, large crosses) corresponding to model outputs of +1 and –1 (that is, choice 1 or 2).

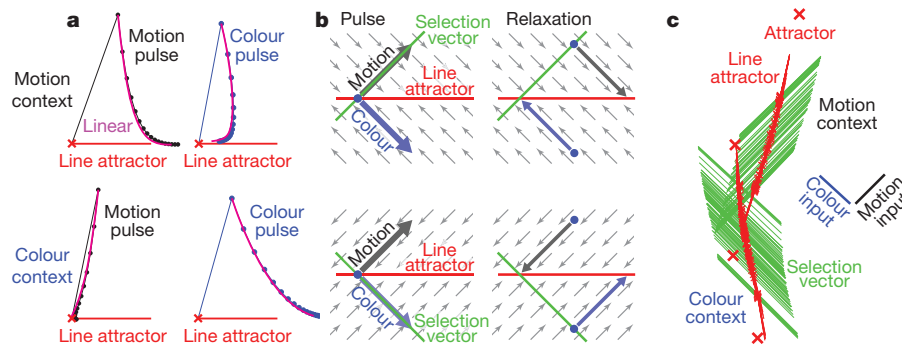


Figure 6 | Selection and integration by recurrent dynamics. **a**, Average model population response to short (1-ms) pulses of motion (left) and colour inputs (right) during motion (top) and colour contexts (bottom). Motion or colour inputs (solid lines) are initiated when the system is steady at one of the identified fixed points (red crosses), and subsequent relaxation back to the line attractor is simulated (dots: 3-ms intervals) and averaged across fixed points. The size of the pulses approximately corresponds to the length of the scale bars in Fig. 5. Selection of the relevant input results from the context-dependent relaxation of the recurrent dynamics after the pulse, and is well approximated by the linearized dynamics around the fixed points (magenta lines). Responses

are projected into the two-dimensional subspace spanned by the direction of the pulse and the locally computed line attractor (the right zero-eigenvector of the linearized dynamics). **b**, Explanation of how the same input pulse (left) leads to evidence integration in one context, but is ignored in the other (right). Relaxation towards the line attractor (small arrows) is always orthogonal to the context-dependent selection vector, and reverses the effects of the irrelevant pulse. **c**, Global arrangement of the line attractor (red) and selection vector (green) at each fixed point. Inputs are selected by the selection vector, which is orthogonal to the contextually irrelevant input (note input axes, right), and integrated along the line attractor.

dynamics, although counterintuitive, nevertheless follow a very simple rule. For a given context, the relaxation always occurs on a path that is orthogonal to a specific direction in state space, which we call the 'selection vector' (Fig. 6b). The direction of the selection vector, like the direction of the line attractor, is a property of the recurrent synaptic weights learned by the model during training (see Supplementary Information). Unlike the line attractor, however, the orientation of the selection vector changes with context—it projects strongly onto the relevant input, but is orthogonal to the irrelevant one (Fig. 6b). As a consequence, the relaxation dynamics around the line attractor are context dependent. This mechanism explains how the same sensory input can result in movement along the line attractor in one context but not the other (Fig. 6b).

The line attractor and the selection vector are sufficient to explain the linearized dynamics around each fixed point (see Supplementary Information), and approximate well the responses of the full model (magenta curves, Fig. 6a). Mathematically, the line attractor and the selection vector correspond to the right and left zero-eigenvector of the underlying linear system. Within a context, these locally defined eigenvectors point in a remarkably consistent direction across different fixed points—the selection vector, in particular, is always aligned with the relevant input and orthogonal to the irrelevant input (Fig. 6c and Extended Data Fig. 10q–s). As a result, the two line attractors (Fig. 6c) show relaxation dynamics appropriate for selecting the relevant input along their entire length.

Discussion

We describe a novel mechanism underlying flexible, context-dependent selection of sensory inputs and their integration towards a choice (see refs 39–41 for related concepts). This mechanism is sufficient to explain the selection and integration of motion inputs in both monkeys, and of colour inputs in monkey A, which are not filtered out by context before they reach PFC.

A randomly initialized, recurrent neural network trained to solve a task analogous to the monkeys' task reproduces the main features of the data, and analysis of the trained network elucidates the novel selection mechanism. Integration along line attractors, and its relation to the selection vector, has been described before³⁹. However, our model demonstrates how a single nonlinear model can implement flexible computations by reconfiguring the selection vector and the corresponding recurrent dynamics based on a contextual input. Counterintuitively, in the model the projection of an input onto the line attractor does

not determine the extent to which it is integrated, a manifestation of 'non-normal' dynamics^{40,42,43} (see Supplementary Information).

Our results show that the modulation of sensory responses is not necessary to select among sensory inputs (see also refs 44–46). Consistent with this conclusion, two studies using tasks similar to ours^{47,48}, as well as our own recordings in the middle temporal visual area (MT) of monkey A (data not shown), have found no evidence for consistent firing rate modulations in the relevant sensory areas. The dynamical process outlined in this paper is fully sufficient for context-dependent selection in a variety of behavioural models^{3–8}, but it need not be exclusive. Multiple selection mechanisms may exist within the brain.

Our results indicate that computations in prefrontal cortex emerge from the concerted dynamics of large populations of neurons, and are well studied in the framework of dynamical systems^{17,19–23,24,39,49}. Notably, the rich dynamics of PFC responses during selection and integration of inputs can be characterized and understood with just two features of a dynamical system—the line attractor and the selection vector, which are defined only at the level of the neural population. This parsimonious account of cortical dynamics contrasts markedly with the complexity of single neuron responses typically observed in PFC and other integrative structures, which reveal multiplexed representation of many task-relevant and choice-related signals^{1,2,15,16,25,26,50}. In light of our results, these mixtures of signals can be interpreted as separable representations at the level of the neural population^{15,17,25,26}. A fundamental function of PFC may be to generate such separable representations, and to flexibly link them through appropriate recurrent dynamics to generate the desired behavioural outputs.

METHODS SUMMARY

Two adult male rhesus monkeys (14 and 12 kg) were trained on a two-alternative, forced-choice, visual discrimination task. While the monkeys were engaged in the behavioural task, we recorded single- and multiunit responses in the arcuate sulcus and the prearcuate gyrus, and in cortex near and lateral to the principal sulcus. The great majority of neurons were not recorded simultaneously, but rather in separate behavioural sessions. All surgical and behavioural procedures conformed to the guidelines established by the National Institutes of Health and were approved by the Institutional Animal Care and Use Committee of Stanford University. We pooled data from single- and multiunit recordings to construct population responses, and used state space analysis to study the effect of task conditions and time on the population responses. We developed a dimensionality reduction technique ('targeted dimensionality reduction') to identify a low-dimensional subspace capturing variance due to the task variables of interest. We compared the recorded responses to the responses of units in a nonlinear, recurrent neural network model. We trained the model (that is, optimized its

synaptic weights with a 'back-propagation' algorithm) to perform a task analogous to the one performed by the monkeys. We then reverse-engineered the model to discover its mechanism of selective integration. We identified fixed points of the model dynamics, linearized the dynamics around the fixed points, and used linear systems analysis to understand the linearized dynamics. Full methods are provided in the Supplementary Information.

Online Content Any additional Methods, Extended Data display items and Source Data are available in the online version of the paper; references unique to these sections appear only in the online paper.

Received 27 September 2012; accepted 8 October 2013.

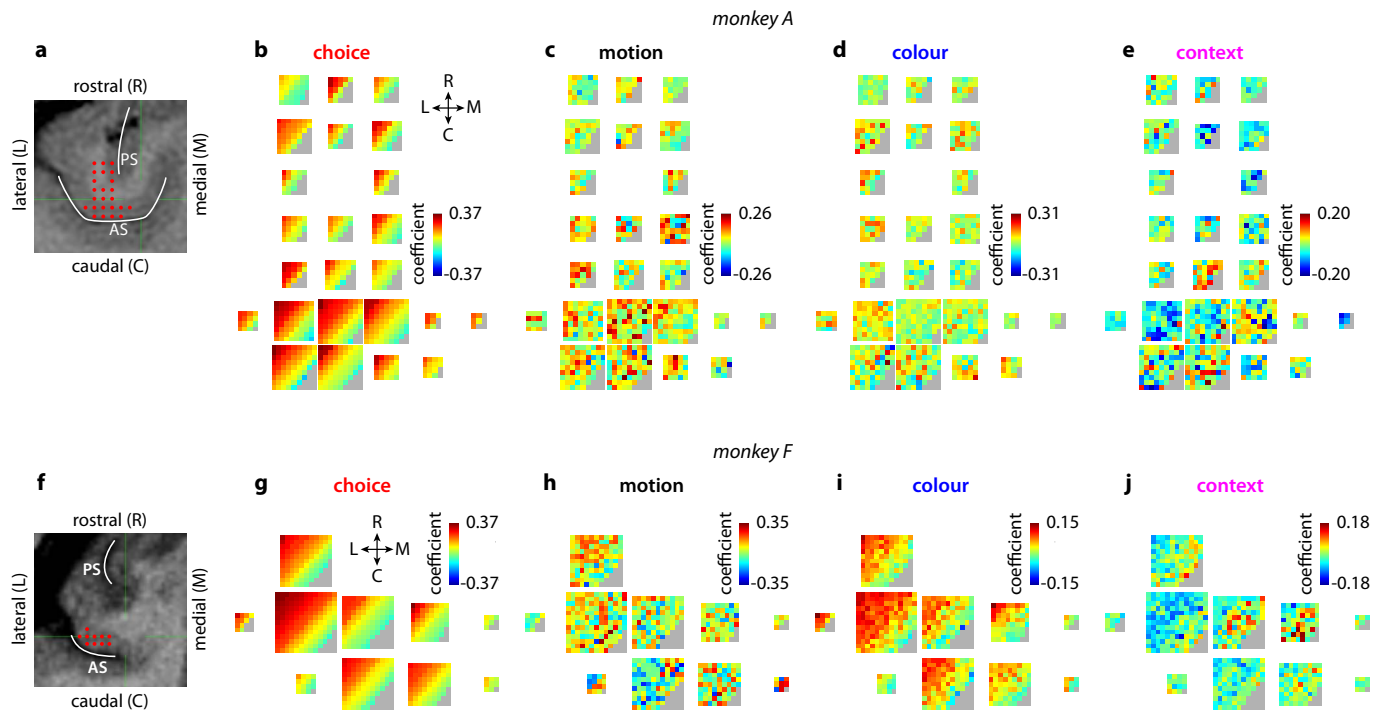
- Fuster, J. M. *The Prefrontal Cortex* 4th edn (Academic, 2008).
- Miller, E. K. & Cohen, J. D. An integrative theory of prefrontal cortex function. *Annu. Rev. Neurosci.* **24**, 167–202 (2001).
- Desimone, R. & Duncan, J. Neural mechanisms of selective visual attention. *Annu. Rev. Neurosci.* **18**, 193–222 (1995).
- Schroeder, C. E. & Lakatos, P. Low-frequency neuronal oscillations as instruments of sensory selection. *Trends Neurosci.* **32**, 9–18 (2009).
- Noudoost, B., Chang, M. H., Steinmetz, N. A. & Moore, T. Top-down control of visual attention. *Curr. Opin. Neurobiol.* **20**, 183–190 (2010).
- Reynolds, J. H. & Chelazzi, L. Attentional modulation of visual processing. *Annu. Rev. Neurosci.* **27**, 611–647 (2004).
- Maunsell, J. H. & Treue, S. Feature-based attention in visual cortex. *Trends Neurosci.* **29**, 317–322 (2006).
- Fries, P. Neuronal gamma-band synchronization as a fundamental process in cortical computation. *Annu. Rev. Neurosci.* **32**, 209–224 (2009).
- Mansouri, F. A., Tanaka, K. & Buckley, M. J. Conflict-induced behavioural adjustment: a clue to the executive functions of the prefrontal cortex. *Nature Rev. Neurosci.* **10**, 141–152 (2009).
- Tanji, J. & Hoshi, E. Role of the lateral prefrontal cortex in executive behavioral control. *Physiol. Rev.* **88**, 37–57 (2008).
- Bruce, C. J. & Goldberg, M. E. Primate frontal eye fields. I. Single neurons discharging before saccades. *J. Neurophysiol.* **53**, 603–635 (1985).
- Schall, J. D. The neural selection and control of saccades by the frontal eye field. *Phil. Trans. R. Soc. Lond. B* **357**, 1073–1082 (2002).
- Moore, T. The neurobiology of visual attention: finding sources. *Curr. Opin. Neurobiol.* **16**, 159–165 (2006).
- Kim, J. N. & Shadlen, M. N. Neural correlates of a decision in the dorsolateral prefrontal cortex of the macaque. *Nature Neurosci.* **2**, 176–185 (1999).
- Machens, C. K., Romo, R. & Brody, C. D. Functional, but not anatomical, separation of "what" and "when" in prefrontal cortex. *J. Neurosci.* **30**, 350–360 (2010).
- Rigotti, M. *et al.* The importance of mixed selectivity in complex cognitive tasks. *Nature* **497**, 585–590 (2013).
- Stokes, M. G. *et al.* Dynamic coding for cognitive control in prefrontal cortex. *Neuron* **78**, 364–375 (2013).
- Hernández, A. *et al.* Decoding a perceptual decision process across cortex. *Neuron* **66**, 300–314 (2010).
- Churchland, M. M. *et al.* Neural population dynamics during reaching. *Nature* **487**, 51–56 (2012).
- Shenoy, K. V., Sahani, M. & Churchland, M. M. Cortical control of arm movements: a dynamical systems perspective. *Annu. Rev. Neurosci.* **36**, 337–359 (2013).
- Stopfer, M., Jayaraman, V. & Laurent, G. Intensity versus identity coding in an olfactory system. *Neuron* **39**, 991–1004 (2003).
- Briggman, K. L., Abarbanel, H. D. & Kristan, W. B. Jr. Optical imaging of neuronal populations during decision-making. *Science* **307**, 896–901 (2005).
- Harvey, C. D., Coen, P. & Tank, D. W. Choice-specific sequences in parietal cortex during a virtual-navigation decision task. *Nature* **484**, 62–68 (2012).
- Afshar, A. *et al.* Single-trial neural correlates of arm movement preparation. *Neuron* **71**, 555–564 (2011).
- Sigala, N., Kusunoki, M., Nimmo-Smith, I., Gaffan, D. & Duncan, J. Hierarchical coding for sequential task events in the monkey prefrontal cortex. *Proc. Natl Acad. Sci. USA* **105**, 11969–11974 (2008).
- Machens, C. K. Demixing population activity in higher cortical areas. *Front. Comput. Neurosci.* **4**, 126 (2010).
- Shadlen, M. N. & Newsome, W. T. Neural basis of a perceptual decision in the parietal cortex (area LIP) of the rhesus monkey. *J. Neurophysiol.* **86**, 1916–1936 (2001).
- Mazurek, M. E., Roitman, J. D., Ditterich, J. & Shadlen, M. N. A role for neural integrators in perceptual decision making. *Cereb. Cortex* **13**, 1257–1269 (2003).
- Wang, X. J. Probabilistic decision making by slow reverberation in cortical circuits. *Neuron* **36**, 955–968 (2002).
- Cohen, J. D., Dunbar, K. & McClelland, J. L. On the control of automatic processes: a parallel distributed processing account of the Stroop effect. *Psychol. Rev.* **97**, 332–361 (1990).
- Deco, G. & Rolls, E. T. Attention and working memory: a dynamical model of neuronal activity in the prefrontal cortex. *Eur. J. Neurosci.* **18**, 2374–2390 (2003).
- Sussillo, D. & Abbott, L. F. Generating coherent patterns of activity from chaotic neural networks. *Neuron* **63**, 544–557 (2009).
- Sussillo, D. & Barak, O. Opening the black box: low-dimensional dynamics in high-dimensional recurrent neural networks. *Neural Comput.* **25**, 626–649 (2013).
- Zipser, D. & Andersen, R. A. A back-propagation programmed network that simulates response properties of a subset of posterior parietal neurons. *Nature* **331**, 679–684 (1988).
- Martens, J. & Sutskever, I. Learning recurrent neural networks with hessian-free optimization. *Proc. 28th Int. Conf. Machine Learn.* (ICML, 2011).
- Churchland, A. K., Kiani, R. & Shadlen, M. N. Decision-making with multiple alternatives. *Nature Neurosci.* **11**, 693–702 (2008).
- Reddi, B. A. & Carpenter, R. H. The influence of urgency on decision time. *Nature Neurosci.* **3**, 827–830 (2000).
- Brunton, B. W., Botvinick, M. M. & Brody, C. D. Rats and humans can optimally accumulate evidence for decision-making. *Science* **340**, 95–98 (2013).
- Seung, H. S. How the brain keeps the eyes still. *Proc. Natl Acad. Sci. USA* **93**, 13339–13344 (1996).
- Goldman, M. S. Memory without feedback in a neural network. *Neuron* **61**, 621–634 (2009).
- Sejnowski, T. J. On the stochastic dynamics of neuronal interaction. *Biol. Cybern.* **22**, 203–211 (1976).
- Murphy, B. K. & Miller, K. D. Balanced amplification: a new mechanism of selective amplification of neural activity patterns. *Neuron* **61**, 635–648 (2009).
- Ganguli, S., Huh, D. & Sompolinsky, H. Memory traces in dynamical systems. *Proc. Natl Acad. Sci. USA* **105**, 18970–18975 (2008).
- Salinas, E. Context-dependent selection of visuomotor maps. *BMC Neurosci.* **5**, 47 (2004).
- Zénon, A. & Krauzlis, R. J. Attention deficits without cortical neuronal deficits. *Nature* **489**, 434–437 (2012).
- Roy, J. E., Riesenhuber, M., Poggio, T. & Miller, E. K. Prefrontal cortex activity during flexible categorization. *J. Neurosci.* **30**, 8519–8528 (2010).
- Sasaki, R. & Uka, T. Dynamic readout of behaviorally relevant signals from area MT during task switching. *Neuron* **62**, 147–157 (2009).
- Katzner, S., Busse, L. & Treue, S. Attention to the color of a moving stimulus modulates motion-signal processing in macaque area MT: evidence for a unified attentional system. *Front. Syst. Neurosci.* **3**, 12 (2009).
- Machens, C. K., Romo, R. & Brody, C. D. Flexible control of mutual inhibition: a neural model of two-interval discrimination. *Science* **307**, 1121–1124 (2005).
- Huk, A. C. & Meister, M. L. Neural correlates and neural computations in posterior parietal cortex during perceptual decision-making. *Front. Integr. Neurosci.* **6**, 86 (2012).

Supplementary Information is available in the online version of the paper.

Acknowledgements We thank J. Powell, S. Fong and J. Brown for technical assistance, L. Abbott, for conversations on non-normal dynamics, and L. Stryer, S. Hohl, S. Ganguli, M. Sahani, R. Kiani, C. Moore and T. Bhattacharya for discussions. V.M. and W.T.N. were supported by HHMI and the Air Force Research Laboratory (FA9550-07-1-0537); D.S. and K.V.S. by a NIH Director's Pioneer Award (1DP10D006409) and DARPA REPAIR (N66001-10-C-2010).

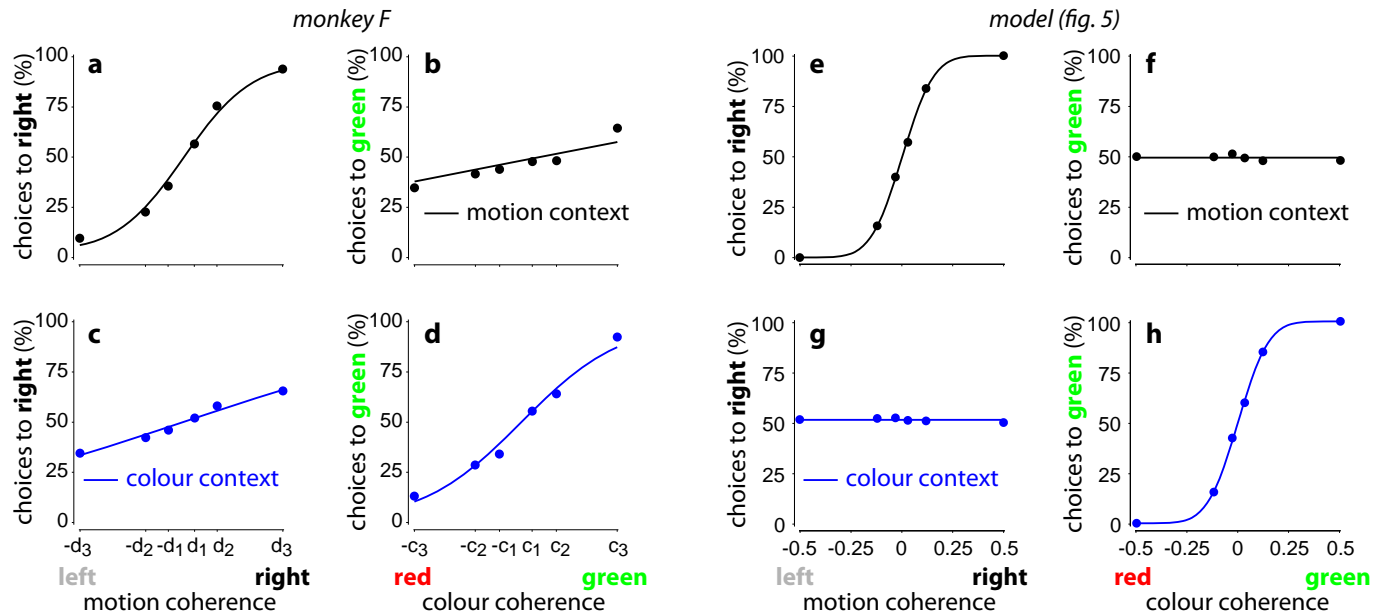
Author Contributions V.M. and W.T.N. designed the study. V.M. collected the data. D.S. implemented the recurrent network. V.M. and D.S. analysed and modelled the data. V.M., D.S., K.V.S. and W.T.N. discussed the findings and wrote the paper.

Author Information Reprints and permissions information is available at www.nature.com/reprints. The authors declare no competing financial interests. Readers are welcome to comment on the online version of the paper. Correspondence and requests for materials should be addressed to V.M. (valerio@ini.phys.ethz.ch) or D.S. (sussillo@stanford.edu).



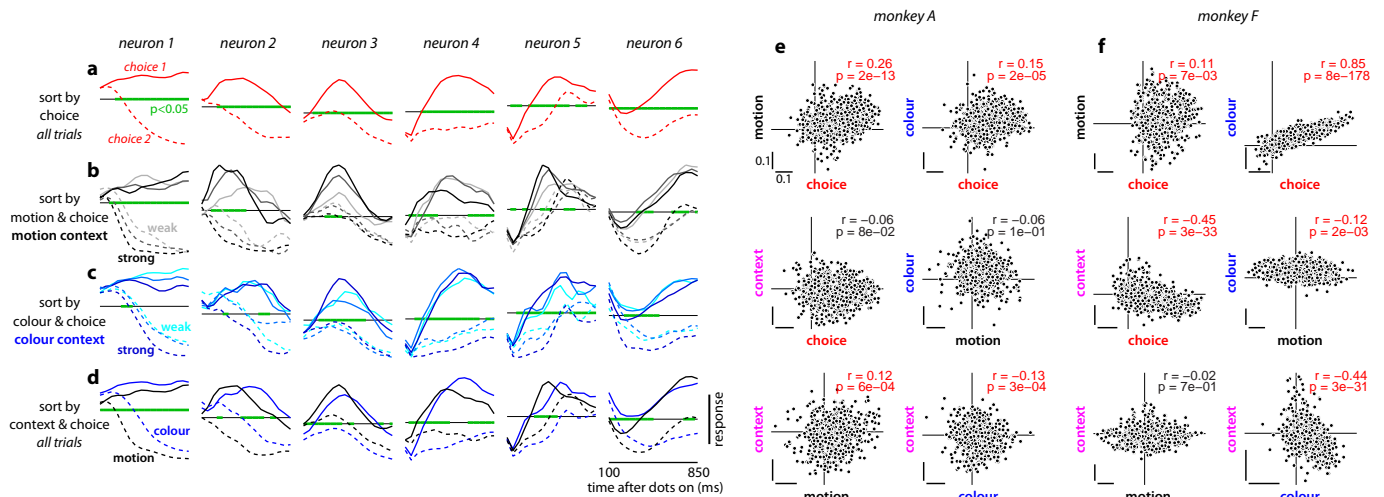
Extended Data Figure 1 | Recording locations and task-related patterns of population activity in PFC. **a**, Recording locations (red dots) in monkey A are shown on anatomical magnetic resonance images in imaging planes that were oriented perpendicularly to the direction of electrode penetrations. Electrodes were lowered through a grid (1-mm spacing) positioned over the arcuate sulcus (AS). Recordings covered the entire depth of the AS and extended rostrally onto the prearcuate gyrus and cortex near and lateral to the principal sulcus (PS). **b–e**, Representation of four task variables in the population response. Each multi-coloured square corresponds to a recording location (red dots) in **a**. Within each square, each pixel corresponds to a unit recorded from that grid position, such that each square represents all the units recorded at the corresponding location. The colour of a pixel indicates the de-noised regression coefficient of choice (**b**), motion coherence (**c**), colour coherence (**d**) and context (**e**) for a given unit (colour bars; grey: no units). These coefficients describe how much the trial-by-trial firing rate of a given unit depends on the task variables in **b–e**. The position of each unit within a square is arbitrary; we therefore sorted them according to the amplitude of the coefficient of choice, which accounts for the diagonal bands of colour in **b** (top-left to bottom-right,

high to low choice coefficient). The positions of the pixels established in **b** are maintained in **c–e**, so that one can compare the amplitude of the coefficient for each task variable for every unit recorded from monkey A. Each of the four panels can be interpreted as the pattern of population activity elicited by the corresponding task variable. The four task variables elicit very distinct patterns of activity and are separable at the level of the population. Importantly, the coefficients were de-noised with principal component analysis (see Supplementary Information, section 6.7) and can be estimated reliably from noisy neural responses (Extended Data Fig. 4i–l). Differences between activation patterns therefore reflect differences in the properties of the underlying units, not noise. **f–j**, Recording locations and task-related patterns of population activity for monkey F. Same conventions as in **a–e**. Recordings (**f**) covered the entire depth of the AS. The patterns of population activity elicited by a choice (**g**), by the motion evidence (**h**) and by context (**j**) are distinct, meaning that the representations of these task variables are separable at the level of the population. The representations of choice (**g**) and colour (**i**), however, are not separable in monkey F, indicating that colour inputs are processed differently in the two monkeys (see main text).



Extended Data Figure 2 | Psychophysical performance for monkey F and for the model. **a–d**, Psychophysical performance for monkey F, for motion (top) and colour contexts (bottom), averaged over 60 recording sessions (123,550 trials). Performance is shown as a function of motion (left) or colour (right) coherence in each behavioural context. As in Fig. 1c–f, coherence values along the horizontal axis correspond to the average low, intermediate and high motion coherence (**a**, **c**) and colour coherence (**b**, **d**) computed over all behavioural trials. The curves are fits of a behavioural model (see Supplementary Information, section 4). **e–h**, ‘Psychophysical’ performance for the trained neural-network model (Figs 4–6) averaged over a total of 14,400 trials (200 repetitions per condition). Choices were generated based on the output of the model at the end of the stimulus presentation—an output larger than zero corresponds to a choice to the left target (choice 1), and an output

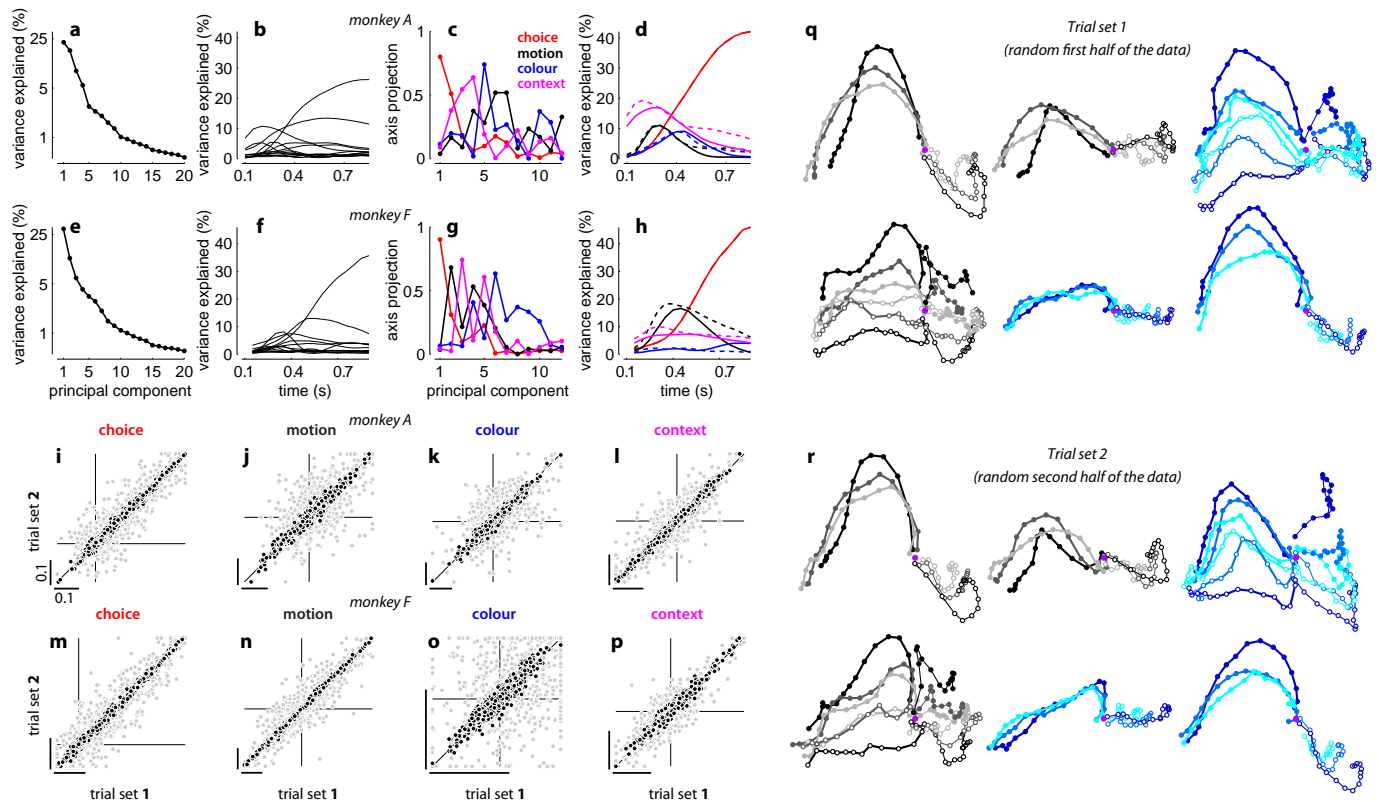
smaller than zero corresponds to a choice to the right target (choice 2). We simulated model responses to inputs with motion and colour coherences of 0.03, 0.12 and 0.50. The variability in the input (that is, the variance of the underlying Gaussian distribution) was chosen such that the performance of the model for the relevant sensory signal qualitatively matches the performance of the monkeys. As in Fig. 1c–f, performance is shown as a function of motion (left) or colour (right) coherence in the motion (top) and colour contexts (bottom). Curves are fits of a behavioural model (as in **a–d** and in Fig. 1c–f). In each behavioural context, the relevant sensory input affects the model’s choices (**e**, **h**), but the irrelevant input does not (**f**, **g**), reflecting successful context-dependent integration. The model output essentially corresponds to the bounded temporal integral of the relevant input (not shown) and is completely unaffected by the irrelevant input.



Extended Data Figure 3 | Mixed representation of task variables in PFC.

a–d, Example responses from six well-isolated single units in monkey A. Each column shows average normalized responses on correct trials for one of the single units. Responses are aligned to the onset of the random-dot stimulus, averaged with a 50-ms sliding window, and sorted by one or more task-related variables (choice, motion coherence, colour coherence, context). The green lines mark time intervals with significant effects of choice (**a**), motion coherence (**b**), colour coherence (**c**), or context (**d**) as assessed by multi-variable, linear regression (regression coefficient different from zero, $P < 0.05$). Linear regression and coefficient significance are computed over all trials (correct and incorrect, motion and colour context; Supplementary Information, section 6.3). The horizontal grey line corresponds to a normalized response equal to zero. **a**, Responses sorted by choice (solid, choice 1; dashed, choice 2) averaged over both contexts. **b**, Responses during motion context, sorted by choice and motion coherence (black to light-grey, high to low motion coherence). **c**, Responses during colour context, sorted by choice and colour coherence (blue to cyan, high to low colour coherence). **d**, Responses sorted by

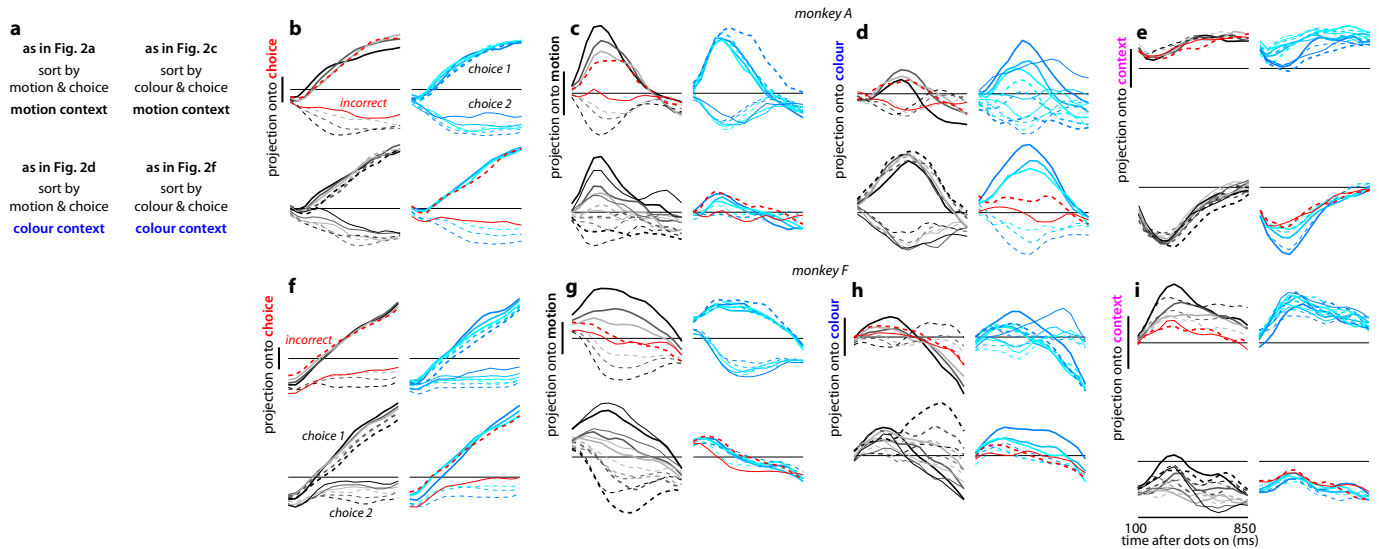
choice and context (black, motion context; blue, colour context). As is typical for PFC, the activity of the example units depends on many task variables, indicating that they represent mixtures of the underlying task variables. **e, f**, De-noised regression coefficients for all units in monkey A (**e**) and monkey F (**f**). The data in Extended Data Fig. 1 are re-plotted here to directly compare the effects of different task variables (choice, motion, colour, context) to each other. Each data point corresponds to a unit, and the position along the horizontal and vertical axes is the de-noised regression coefficient for the corresponding task variable. The horizontal and vertical lines in each panel intersect at the origin (0,0). Scale bars span the same range (0.1) in each panel. The different task variables are mixed at the level of individual units. Although units modulated by only one of the task variables do occur in the population, they do not form distinct clusters but rather are part of a continuum that typically includes all possible combinations of selectivities. Significant correlations between coefficients are shown in red ($P < 0.05$, Pearson's correlation coefficient r).



Extended Data Figure 4 | Targeted dimensionality reduction of population responses, and reliability of task-related axes and population trajectories.

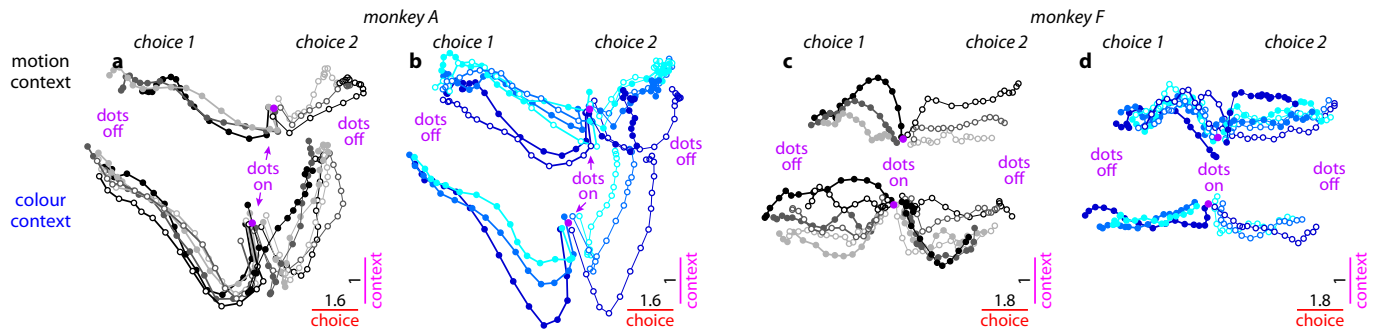
a, Fraction of variance explained by the first 20 principal components of the responses in monkey A. Principal components are computed on correct trials only, on condition-averaged responses. Conditions are defined on the basis of choice, motion coherence, colour coherence and context. Each time point of the average response for a given condition contributes an ‘independent’ sample for the principal components analysis, and variance is computed over conditions and times. **b**, Fraction of variance explained by the first 12 principal components. The total explainable variance (100%) is computed separately at each time, and reflects response differences across conditions. **c**, The four ‘task-related axes’ of choice, motion, colour and context expressed as linear combinations of the first 12 principal components. The four axes span a subspace containing the task-related variance in the population response (for example, Fig. 2 and Extended Data Fig. 6) and are obtained by orthogonalizing the de-noised regression vectors for the corresponding task variables (see Supplementary Information, section 6.7; de-noised regression coefficients are shown in Extended Data Figs 1 and 3e, f). The vertical axis in **c** corresponds to the projection of each axis onto a given principal component (that is, the contribution of that principal component to each axis). All four axes project onto multiple principal components and thus the corresponding task variables are mixed at the level of single principal components. **d**, Fraction of variance explained by the task-related axes of choice, motion, colour and context (solid lines), as in **b**. The four axes explain a larger fraction of the variance than the principal components at many times but, unlike the principal components, they do not explain the variance common to all conditions that is due to the passage of time (not shown). A possible concern with our analysis is that the time courses of variance explained in **d** could be misleading if the task-related axes, which we estimated only at a single time for each variable, are changing over time during the presentation of the random dots. Under this scenario, for example, the ‘humped’ shape of the motion input (solid black trace) might reflect a changing ensemble code for motion rather than actual changes in the strength of the motion signal in the neural population. To control for this possibility, we also computed time-varying ‘task-related axes’ by estimating the axes of motion, colour and context separately at each time throughout the 750-ms dots presentation. The fractions of variance explained by the time-varying axes (dashed lines) and by the fixed axes (solid lines) have similar amplitudes and time courses. Thus, the effects of the corresponding task variables (during the presentation of the random dots) are adequately captured by the subspace spanned by the fixed axes (see Supplementary Information,

section 6.8). **e–h**, Same as **a–d**, for monkey F. As shown in Extended Data Figs 1g, i and 3f (top-right panel) the de-noised regression coefficients of colour and choice are strongly correlated. As a consequence, the axis of colour explains only a small fraction of the variance in the population responses (**h**, blue; see main text). **i–l**, Reliability of task-related axes in monkey A. To determine to what extent variability (that is, noise) in single unit responses affects the task-related axes of choice, motion, colour and context (for example, Fig. 2 and Extended Data Fig. 6), we estimated each axis twice from two separate sets of trials (trial sets 1 and 2 in **i–l**). For each unit, we first assigned each trial to one of two subsets, and estimated de-noised regression coefficients for the task variables separately for the two subsets. We then obtained task-related axes by orthogonalizing the corresponding de-noised coefficients (see Supplementary Information, section 6.9). Here, the orthogonalized coefficients are computed both with (black) and without (grey) PCA-based de-noising. The horizontal and vertical lines in each panel intersect at the origin (0,0). Scale bars span the same range (0.1) in each panel. Data points lying outside the specified horizontal or vertical plotting ranges are shown on the corresponding edges in each panel. **i**, Coefficients of choice. Each data point corresponds to the orthogonalized coefficient of choice for a given unit, computed from trials in set 1 (horizontal axis) or in set 2 (vertical axis). **j–l**, Same as **i** for the orthogonalized coefficients of motion (**j**), colour (**k**) and context (**l**). **m–p**, Orthogonalized regression coefficients for monkey F, as in **i–l**. Overall, after de-noising the orthogonalized coefficients are highly consistent across the two sets of trials. Therefore, the observed differences in the activation pattern elicited by different task variables (Extended Data Fig. 1) are not due to the noisiness of neural responses, but rather reflect differences in the properties of the underlying units. **q, r**, Reliability of population trajectories. To assess the reliability of the trajectories in Fig. 2, we estimated the task-related axes and the resulting population trajectories (same conventions as Fig. 2) twice from two separate sets of trials (as **i–l**, see Supplementary Information, section 6.9). As in the example trajectories shown in **q** (trial set 1) and **r** (trial set 2), we consistently obtained very similar trajectories across the two sets of trials. To quantify the similarity between the trajectories from the two sets, we used trajectories obtained from one set to predict the trajectories obtained from the other set (see Supplementary Information, section 6.9). On average across 20 randomly defined pairs of trial sets, in both monkeys the population responses from one set explain 94% of the total variance in the responses of the other set (95% for the example in **q** and **r**). These numbers provide a lower bound on the true reliability of trajectories in Fig. 2, which are based on twice as many trials as those in **q** and **r**.



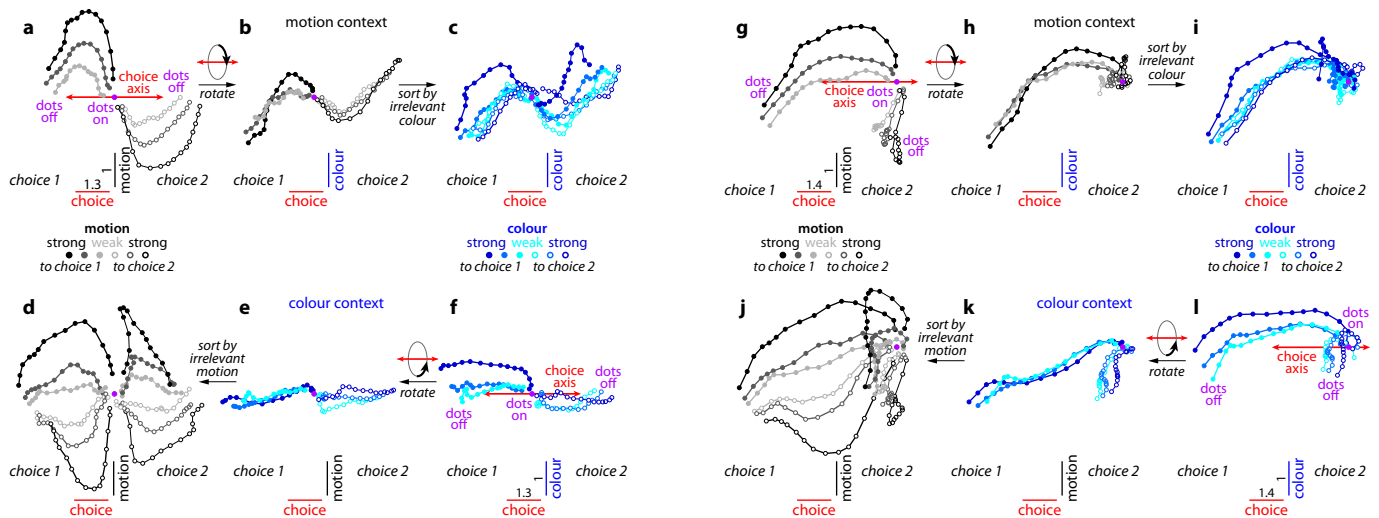
Extended Data Figure 5 | Population responses along individual task-related axes. **a–e**, Responses for monkey A. The average population responses on correct trials are re-plotted from Fig. 2, together with responses on a subset of incorrect trials (red curves). Here the responses are represented explicitly as a function of time (horizontal axis) and projected separately (vertical axes) onto the axes of choice (**b**), motion (**c**), colour (**d**) and context (**e**). As in Fig. 2, correct trials are sorted on the basis of context (motion: top sub-panels; colour: bottom sub-panels; see key in **a**), on the direction of the sensory evidence (filled, towards choice 1; dashed, towards choice 2) and strength of the sensory evidence (black to light-grey, strongest to weakest motion; blue to cyan, strongest to weakest colour), and based on choice (thick, choice 1; thin, choice 2). Incorrect trials (red curves) are shown for the lowest motion coherence (during motion context, top left in **b–e**) and the lowest colour coherence (during colour context, bottom right in **b–e**). Vertical scale bars correspond to 1 unit of normalized response, and the horizontal lines are drawn at the same level in all four sub-panels within **b–e**. **a**, Key to the condition averages shown in each panel of **b–e**, as well as to the corresponding state-space

panels in Fig. 2. **b**, Projections of the population response onto the choice axis. Responses along the choice axis represent integration of evidence in both contexts. **c**, Projection onto the motion axis. Responses along the motion axis represent the momentary motion evidence during both motion (top left) and colour contexts (bottom left) (curves are parametrically ordered based on motion strength in both contexts), but not the colour evidence (right, curves are not ordered based on colour strength). **d**, Projection onto the colour axis. Responses along the colour axis represent the momentary colour evidence in the motion (top right) and colour contexts (bottom right) (ordered), but not the motion evidence (left, not ordered). **e**, Projection onto the context axis. Responses in the motion context (top, all curves above the horizontal line) and colour context (bottom, all curves below the horizontal line) are separated along the context axis, which maintains a representation of context. **f–i**, Responses for monkey F, same conventions as in **b–e**. The responses in **f–i** are also shown as trajectories in Extended Data Fig. 7g–l. The drift along the choice axis in Extended Data Fig. 7g–l is reflected in the overall positive slopes in **f**.



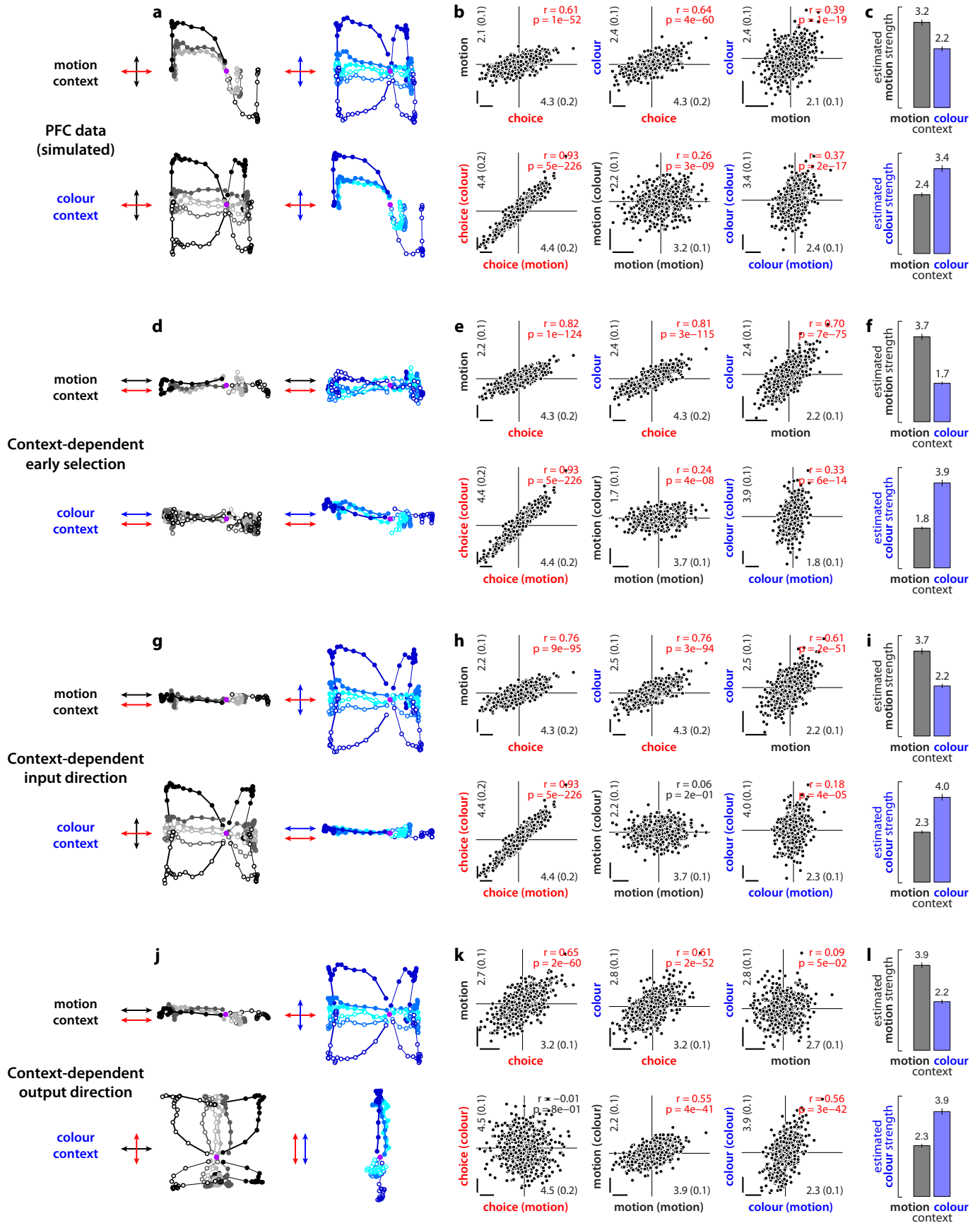
Extended Data Figure 6 | Effect of context on PFC dynamics. **a, b,** Responses from monkey A. Same conditions and conventions as in Fig. 2, but for activity projected into the two-dimensional subspace capturing the variance due to choice (along the choice axis) and context (context axis). Components along the choice axis are enhanced relative to the context axis (see scale bars). The population response contains a representation of context, which is reflected in the separation between trajectories in the motion and colour contexts along the axis of context. The contextual signal is strongest early during the dots presentation. **a,** Effects of context (motion context versus colour context),

choice (choice 1 versus choice 2), and motion input (direction and coherence, grey colours). **b,** Same trials as in **a,** but averaged to show the effect of the colour input (blue colours). **c, d,** Responses from monkey F, same conventions as in **a, b.** As in Extended Data Fig. 7a–f, we subtracted the across-condition average trajectory from each individual, raw trajectory (see Supplementary Information, section 6.10). The underlying raw population responses are shown in Extended Data Fig. 5f–i, and confirm that the representation of context is stable throughout the dots presentation time (Extended Data Fig. 5i).



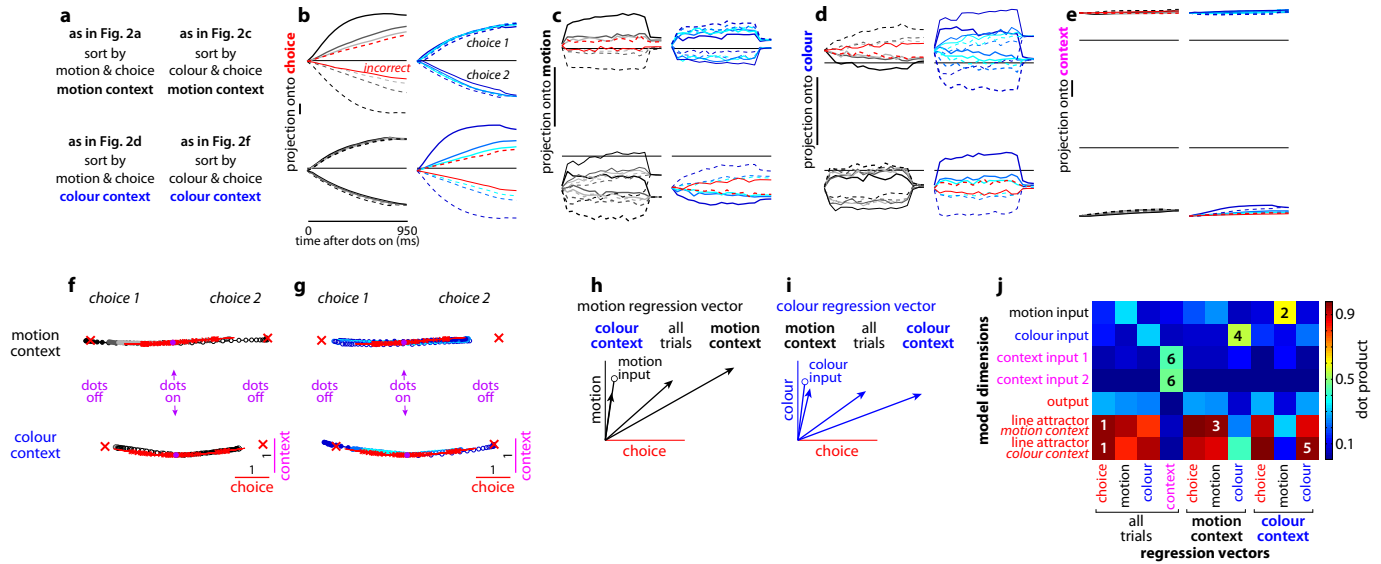
Extended Data Figure 7 | Dynamics of population responses in monkey F. **a–f**, Response trajectories in the subspace spanned by the task-related axes of choice, motion and colour. Same conventions as in Fig. 2. Unlike in Fig. 2, here we subtracted the across-condition average trajectory from each individual, raw trajectory (see Supplementary Information, section 6.10). The raw trajectories are shown in **g–l** and the corresponding projections onto individual axes in Extended Data Fig. 5f–i. Three key features of the population responses are shared in monkey A (Fig. 2) and monkey F. First, movement along a single choice axis (**a** and **f**, red arrows) corresponds to integration of the relevant evidence in both contexts. Second, in both contexts the momentary motion evidence elicits responses along the axis of motion, which is substantially different from the axis of choice (**a** and **d**). Third, the motion evidence is strongly represented whether it is relevant (**a**) or irrelevant (**d**). Thus, the processing of motion inputs in both monkeys is inconsistent with current models of selection and integration (Fig. 3b–d). Unlike in monkey A, responses along the colour axis in monkey F (**f** and **c**) reflect the momentary colour evidence only weakly. The effects of colour on the trajectories in monkey F

resemble the responses expected by the early selection model (Fig. 3b). **g–l**, Raw population responses. Population trajectories were computed and are represented as in Fig. 2. The trajectories in **a–f** were obtained by subtracting the across-condition average from each individual trajectory shown above. Overall, the responses have a tendency to move towards the left along the choice axis. An analogous, although weaker, overall drift can also be observed in monkey A, and contributes to the asymmetry between trajectories on choice 1 and choice 2 trials (Fig. 2). Because choice 1 corresponds to the target in the response field of the recorded neurons (see Supplementary Information, section 6.2), the drift reflects a tendency of individual firing rates to increase throughout the stimulus presentation time. By the definition of choice 1 and choice 2, a similar but opposite drift has to occur in neurons whose response field overlaps with choice 2 (the responses of which we did not record). In the framework of diffusion-to-bound models, such a drift can be interpreted as an urgency signal, which guarantees that the decision boundary is reached before the offset of the dots (refs 36, 37).



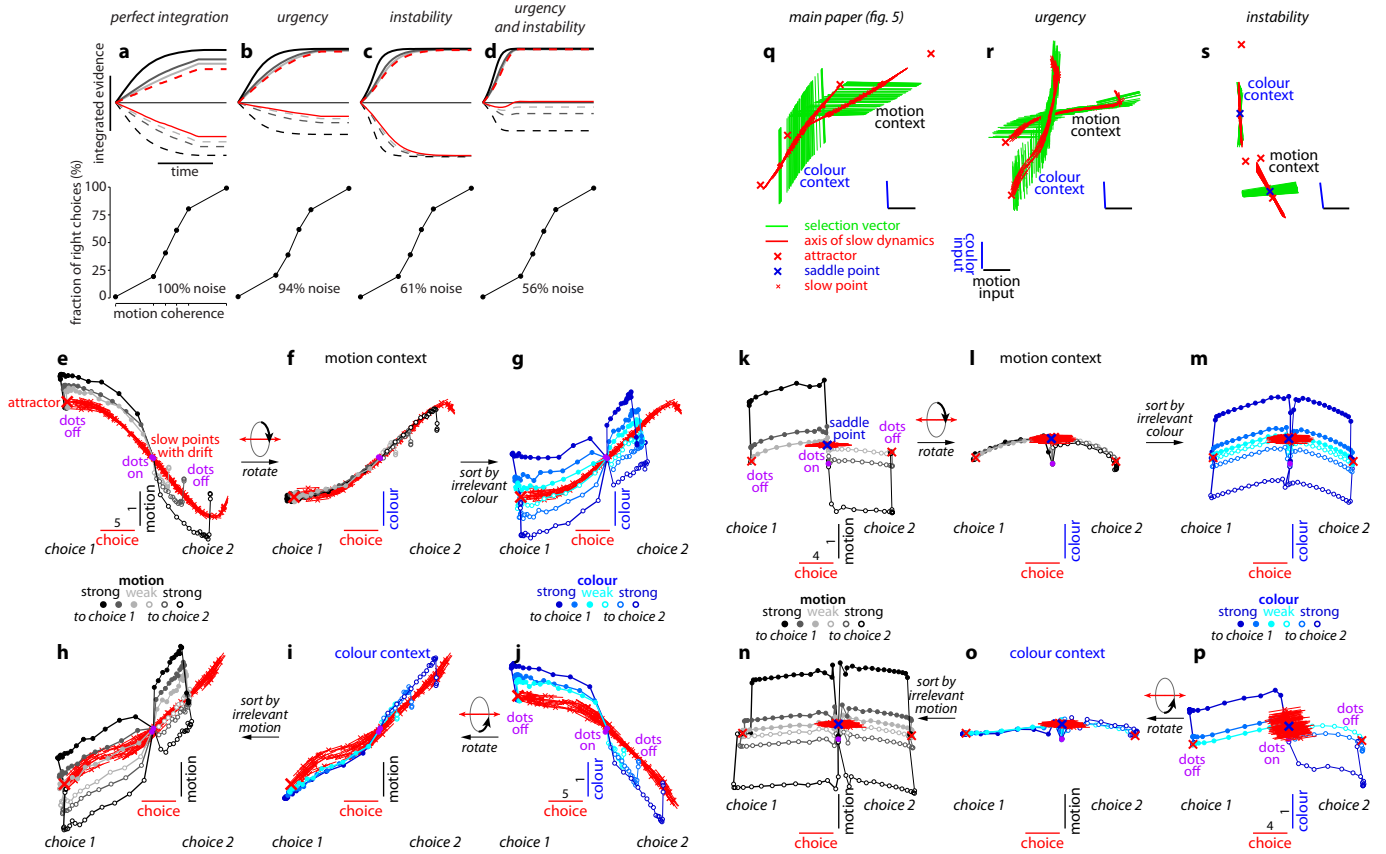
Extended Data Figure 8 | Simulations of models of selective integration inconsistent with PFC responses. We simulated population responses mimicking the observed PFC responses (a–c) and alternative responses expected based on the three models of context-dependent selection described in Fig. 3b–d (d–l) (see Supplementary Information, section 8). These simulations are based on a diffusion-to-bound model, unlike the simulations of the recurrent neural network models in Figs 5 and 6 and in Extended Data Figs 9 and 10e–s. Here, single neurons represent mixtures of three time-dependent task variables of a diffusion-to-bound model, namely the momentary motion and colour evidence and the integrated relevant evidence. At the level of the population, these three task variables are represented along specific directions in state space (arrows in a, d, g, j; red, integrated evidence; black, momentary motion evidence; blue, momentary colour evidence). The four simulations differ only with respect to the direction and context dependence of the three task variables. We computed state space trajectories from the population responses using the targeted dimensionality reduction techniques discussed in the main text and in Supplementary Information. The resulting simulated population responses reproduce the schematic population responses in Fig. 3. a–c, Simulated population responses mimicking the observed PFC responses (Fig. 2). a, Response trajectories in the two-dimensional subspace capturing the effects of choice and motion (left) or choice and colour (right) in the motion (top) and colour (bottom) contexts. Same conditions and conventions as in Fig. 2a, c and Fig. 2d, f. The three task variables are represented along three orthogonal directions in state space (arrows). b, Regression coefficients of choice, motion and colour for all simulated units in the population. For each

unit, coefficients were computed with linear regression on all simulated trials (top) or separately on trials from the motion or colour context (bottom, context in parentheses). Scale bars represent arbitrary units. Numbers in the inset along each axis represent averages of the absolute value of the corresponding coefficients (\pm s.e.m., in parentheses). Significant correlations between coefficients are shown in red ($P < 0.05$, Pearson's correlation coefficient r). c, Estimated strengths of the motion (top) and colour (bottom) inputs during motion (black) and colour (blue) contexts. Input strength is defined as the average of the absolute value of the corresponding regression coefficients. d–f, same as a–c, for simulated population responses expected from context-dependent early selection (Fig. 3b). When relevant, momentary motion (top) and colour (bottom) evidence are represented along the same direction as integrated evidence (arrows in d). g–i, same as a–c, for simulated population responses expected from context-dependent input directions (Fig. 3c). Integrated evidence is represented along the same direction in both contexts (red arrows in g). The relevant momentary evidence (motion in the motion context, top; colour in the colour context, bottom) is aligned with the direction of integration, whereas the irrelevant momentary evidence is orthogonal to it (black and blue arrows in g). j–l, same as a–c, for simulated population responses expected from context-dependent output directions (Fig. 3d). The momentary motion and colour evidence are represented along the same directions in both contexts (black and blue arrows in j). The direction of integration (red arrows in j) is aligned with the motion evidence in the motion context (top), and with the colour evidence in the colour context (bottom).



Extended Data Figure 9 | Model population responses and validation of targeted dimensionality reduction. **a–e**, Model population responses along individual task-related axes, same conventions as in Extended Data Fig. 5. Here we defined the task-related axes directly based on the synaptic connectivity in the model (see Supplementary Information, section 7.6; and panels **h–j**), rather than using the approximate estimates based on the population response (as for the PFC data, for example, Fig. 2). The same axes and the resulting projections underlie the trajectories in Fig. 5. The model integrates the contextually relevant evidence almost perfectly, and the responses along the choice axis (**b**) closely match the output of an appropriately tuned diffusion-to-bound model (not shown). Notably, near-perfect integration is not a core feature of the proposed mechanism of context-dependent selection (see main text, and Extended Data Fig. 10). **f, g**, Effect of context on model dynamics, same conditions and conventions as in Extended Data Fig. 6. Network activity is projected onto the two-dimensional subspace capturing the variance due to choice (along the choice axis) and context (context axis). Same units on both axes (see scale bars). As in Fig. 5, fixed points of the dynamics (red crosses) and the associated right zero-eigenvectors (that is, the local direction of the line attractor, red lines) were computed separately for motion (top) and colour contexts (bottom) in the absence of sensory inputs. The line attractors computed in the two contexts, and the corresponding population trajectories, are separated along the context axis. **f**, Effects of context (motion context, colour context), choice (choice 1, choice 2) and motion input (direction and coherence, grey colours) on the population trajectories. **g**, Same trials as in **f**, but re-sorted and averaged to show the effect of the colour input (blue colours). The context axis is approximately orthogonal to the motion and colour inputs, and thus the effects of motion and colour on the population response (Fig. 5) are not revealed in the subspace spanned by the choice and context axes (**f** and **g**). **h–j**, Validation of targeted dimensionality reduction. To validate the dimensionality reduction approach used to analyse population responses in PFC (see Supplementary Information, sections 6.5–6.7), we estimated the regression vectors of choice, motion, colour and context from the simulated population responses (Fig. 5 and panels **b–g**) and compared them to the exactly known model dimensions that underlie the model dynamics (see definitions below). We estimated the regression vectors in three ways: by pooling responses from all model units and all trials (as in the PFC data, for example, Fig. 2 and Extended Data Fig. 6), or separately

from the motion- and colour-relevant trials (contexts). Orthogonalization of the regression vectors yields the task-related axes of the subspace of interest (for example, axes in Fig. 2). Most model dimensions (motion, colour and context inputs, and output) were defined by the corresponding synaptic weights after training. The line attractor, on the other hand, is the average direction of the right zero-eigenvector of the linearized dynamics around a fixed point, and was computed separately for the motion and colour contexts. **h**, The three regression vectors of motion (black arrows), plotted in the subspace spanned by the choice axis (that is, the regression vector of choice) and the motion axis (that is, the component of the regression vector of motion orthogonal to the choice axis). In the colour context, the motion regression vector closely approximates the actual motion input (black circle—the model dimension defined by synaptic weights). During the motion context, however, the motion regression vector has a strong component along the choice axis, reflecting the integration of motion evidence along that axis. The motion regression vector estimated from all trials corresponds to the average of the vectors from the two contexts; thus all three motion regression vectors lie in the same plane. **i**, The three regression vectors of colour (blue arrows) plotted in the subspace spanned by the choice and colour axes, analogous to **h**. The colour regression vector closely approximates the actual colour input (blue circle) in the motion context, but has a strong component along the choice axis in the colour context. Components along the motion (**h**) and colour (**i**) axes are scaled by a factor of 2 relative to those along the choice axis. **j**, Dot products (colour bar) between the regression vectors (horizontal axis) and the actual model dimensions (vertical axis), computed after setting all norms to 1. The choice regression vector closely approximates the direction of the line attractor in both contexts (squares labelled '1'). As shown also in **h** and **i**, the input regression vectors approximate the model inputs (defined by their synaptic weights) when the corresponding inputs are irrelevant (squares 2 and 4, motion and colour), whereas they approximate the line attractor when relevant (squares 3 and 5). Thus, the motion input is mostly contained in the plane spanned by the choice and motion axes (**h**), and the colour input is mostly contained in the plane spanned by the choice and colour axes (**i**). Finally, the single context regression vector is aligned with both context inputs (squares labelled 6), and closely approximates the difference between the two (not shown).



Extended Data Figure 10 | Urgency and instability in the integration

process. a–d, Choice predictive neural activity (top) and psychometric curves (bottom) predicted by several variants of the standard diffusion-to-bound model (see Supplementary Information, section 7.7). **a**, Standard diffusion-to-bound model. Noisy momentary evidence is integrated over time until one of two bounds (+1 or -1; choice 1 or choice 2) is reached. The momentary evidence at each time point is drawn from a Gaussian distribution whose mean corresponds to the coherence of the input, and whose fixed variance is adjusted in each model to achieve the same overall performance (that is, similar psychometric curves, bottom panels). Coherences are 6%, 18% and 50% (the average colour coherences in monkey A, Fig. 1b). Average integrated evidence (neural firing rates, arbitrary units) is shown on choice 1 and choice 2 trials (thick versus thin) for evidence pointing towards choice 1 or choice 2 (solid versus dashed), on correct trials for all coherences (light grey to black, low to high coherence), and incorrect trials for the lowest coherence (red). The integrated evidence is analogous to the projection of the population response onto the choice axis (for example, Extended Data Fig. 5b, top left and bottom right). **b**, Urgency model. Here the choice is determined by a race between two diffusion processes (typically corresponding to two hemispheres), one with bound at +1, the other with bound at -1. The diffusion in each process is subject to a constant drift towards the corresponding bound, in addition to the drift provided by the momentary evidence. The input-independent drift implements an ‘urgency’ signal, which guarantees that one of the bounds is reached within a short time. Only the integrated evidence from one of the diffusion processes is shown. The three ‘choice 1’ curves are compressed (in contrast to **a**) because the urgency signal causes the bound to be reached, and integration towards choice 1 to cease, more quickly than in **a**. In contrast, the ‘choice 2’ curves are not compressed as the diffusion process that accumulates evidence towards choice 1 never approaches a bound on these trials. **c**, Same as **a**, but here the diffusion process is subject to a drift away from the starting point (0) towards the closest bound (+1 or -1). The strength of the drift is proportional to the distance from the starting point, and creates an ‘instability’ at the starting point. **d**, Same as **b**, with an instability in the integration as in **c** for both diffusion processes. The asymmetry between choice 1 and choice 2 curves in **b** and **d** resembles the asymmetry in the corresponding PFC curves (Extended Data Figs 5b, f, upper left). **e–j**, Neural network model with urgency. This model is based on a similar architecture as the model in Fig. 4. Unlike the neural network in Fig. 4, which was trained solely based on the model output on the last time bin of the trial, here the network is trained based on the output it produces throughout the entire input presentation. The network was trained to reproduce the integrated evidence (that is, the decision variable) for one of the two diffusion processes (that is, one of the two ‘hemispheres’) in a diffusion-to-bound model with urgency (**b**, see Supplementary Information, section 7.7). Similar conventions as in Fig. 5. The urgency signal is controlled by an additional binary input into the network.

Here, the urgency and sensory inputs are turned off as soon as a bound is reached. The network generates only a single, stable fixed point in each context, corresponding to the decision boundary (large red cross). The model also implements a series of points of relatively slow dynamics (small red crosses) approximately lying on a single curve. The axes of slow dynamics at these slow points (red lines) are locally aligned. Notably, responses at these slow points have a strong tendency to drift towards the single, stable fixed point (the decision boundary), and thus the curve of slow points does not correspond to an approximate line attractor. This drift implements the urgency signal and causes an asymmetry in the trajectories, which converge on a single point for choice 1, but have endpoints that are parametrically ordered by coherence along the choice axis for choice 2. As discussed below (panel **r**), this model relies on the same mechanism of selection as the original model (Fig. 5, see main text). **k–p**, Neural network model with instability. Trajectories show simulated population responses for a model (same architecture as in Fig. 4) that was trained to solve the context-dependent task (Fig. 1) only on high-coherence stimuli and in the absence of internal noise (see Supplementary Information, section 7.7). Same conventions as in Fig. 5. In the absence of noise, prolonged integration of evidence is not necessary for accurate performance on the task. As a consequence, the model implements a saddle point (blue cross) instead of an approximate line attractor. Points of slow dynamics (small red crosses, obscured by the red lines) occur only close to the saddle point. The right zero-eigenvectors of the linearized dynamics around these slow points (red lines) correspond to the directions of slowest dynamics, and determine the direction of the axis of choice. When displaced from the saddle point, the responses quickly drift towards one of the two stable attractors (large red crosses) corresponding to the choices. For a given choice, trajectories for all coherences therefore end in the same location along the choice axis, in contrast to the responses in the original model (Fig. 5). Despite these differences, the original model (Fig. 5) and the network model with instability (**k–p**) rely on a common mechanism of context-dependent selection (see panel **s**). **q–s**, Dynamical features (key, bottom) underlying input selection and choice in three related neural network models. All models are based on a common architecture (Fig. 4) but are the result of different training procedures. **q**, Dynamical features of the model described in the main paper (Figs 5 and 6), re-plotted from Fig. 6c. **r**, The urgency model (**e–j**). **s**, The instability model (**k–p**). In all models, the developing choice is implemented as more or less gradual movement along an axis of slow dynamics (specified by the locally computed right eigenvectors associated with the near-zero eigenvalue of the linearized dynamics, red lines). The inputs are selected, that is, result in movement along the axis of slow dynamics, depending on their projection onto the selection vector (the locally computed left eigenvectors associated with the near-zero eigenvalue). In this sense, the three models implement the same mechanisms of context-dependent selection and choice.